Electrical transport properties of microcrystalline silicon grown by plasma enhanced chemical vapor deposition

Nicola Pinto,[a] Marco Ficcadenti, Lorenzo Morresi, and Roberto Murri
INFM-Dipartimento di Fisica, Università di Camerino, Via Madonna delle Carceri, 62032 Camerino, Italy

Giuseppina Ambrosone and Ubaldo Coscia
INFM-Dipartimento di Scienze Fisiche, Università di Napoli "Federico II", Via Cintia, 80126 Napoli, Italy

(Received 24 May 2004; accepted 13 September 2004)

The dark conductivity and Hall mobility of hydrogenated silicon films deposited varying the silane concentration $f=SiH_4/(SiH_4+H_2)$ in a conventional plasma enhanced chemical vapor deposition system have been investigated as a function of temperature, taking into account their structural properties. The electrical properties have been studied in terms of a structural two-phase model. A clear transition from the electrical transport governed by a crystalline phase, in the range $1\% \leqslant f \leqslant 3\%$, to that controlled by an amorphous phase, for $f>3\%$, has been evidenced. Some metastable effects of the dark conductivity have been noticed. © *2004 American Institute of Physics*. [DOI: 10.1063/1.1812818]

I. INTRODUCTION

Hydrogenated microcrystalline silicon, μc-Si:H, was prepared by plasma enhanced chemical vapor deposition (PECVD) several years ago,[1] but only recently it has been used as an intrinsic layer for thin film solar cells and thin film transistors.[2,3] μc-Si:H material is usually grown starting from silane (SiH_4) highly diluted in hydrogen (H_2). In fact, a transition from amorphous to microcrystalline phase is induced when the silane concentration, $f=SiH_4/(SiH_4+H_2)$, is lower than 10%.[4]

The aim of this work was to investigate the electronic transport properties of intrinsic μc-Si:H, because they play a main role in any kind of electronic devices. In this paper we present the results on the electrical characterization of a set of films deposited in a conventional rf PECVD system varying the silane concentration f. The dependence of the conductivity on f was studied according to the observed clear transition from microcrystalline to amorphous phase.

The Hall mobility was measured in films with higher crystallinity degree.

II. EXPERIMENT

We deposited hydrogenated silicon films starting from a gas mixture of silane and hydrogen (SiH_4+H_2) in a high-vacuum PECVD system,[5,6] operating at a frequency of 13.56 MHz, with a constant rf power of 10 W (power density: 67 mW cm^{-2}). The other deposition parameters are quoted in Table I. The substrates were glass (Corning 7059) and monocrystalline silicon wafers for optical, electrical, and structural measurements.

The IR absorption (400–4000 cm^{-1}) measurements were performed by using a Perkin Elmer Spectrum 2000 Fourier transform infrared spectrophotometer to analyze the bond structure of the films. X-ray diffraction (XRD) spectra, measured in the grazing incident mode, were obtained by an X-Pert-MPD (Philips) diffractometer using Cu-Kα radiation to investigate the film structure. The patterns were acquired by a ϑ-2ϑ goniometer mounted on the line shape radiation and equipped with a monochromator, a programmable receiving slit, and a Xe-filled proportional detector. Crystallite sizes were determined by a Debye-Scherrer formula.

The electrical conductivity was measured by means of an electrometer (Keithley 617) in the V/I configuration with an input impedance greater than 10^{16} Ω. Two Au contacts (5 mm apart) were evaporated onto the outer surface of the samples and thermally treated at 450 K for 1 h in vacuum, at $P<10^{-4}$ Pa. An ultrasonic welder soldered fine gold wires to Au strips. The samples were inserted in a small furnace evacuated to $\approx 10^{-4}$ Pa and a completely automatic system was used to measure the conductivity and the Hall mobility as a function of the temperature T. The data acquisition started only when the error on settled temperature was less than ±0.5 K. When necessary, the measurements were done

TABLE I. From left to right the quoted quantities are $f=SiH_4/(SiH_4+H_2)$ ratio; estimated thickness of the films; conductivity activation energies in the high ($E_{\sigma 1}$) and low ($E_{\sigma 2}$) temperature regions, respectively. Other deposition parameters are kept constant: discharge pressure of 133 Pa and rf power of 10 W; substrate temperature of 350 °C.

Sample	f (%)	Thickness (μm)	$E\sigma 1$ (meV)	$E\sigma 2$ (meV)
397	1	0.40	46	148
402	2	0.75	40	126
401	3	0.95	38	141
400	4	0.70	204	635
399	5	0.80	206	590
396	6	0.95	163	592

[a]Author to whom correspondence should be addressed; FAX: +39 0737 402853; electronic mail: nicola.pinto@unicam.it

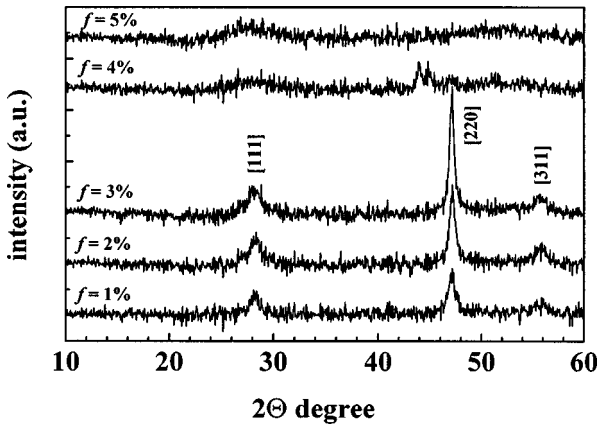

FIG. 1. X-ray diffraction (XRD) spectra for Si films with different f values.

in two different but consecutive runs: the first one starting from room temperature (RT) and going to high temperature (heating) and the second one coming back to RT (cooling). We always measured under slow heating or cooling conditions: in fact, the temperature rate can be estimated to about 2×10^{-2} K/s. Each point of the experimental conductivity curves was computed by averaging at least 50 values.

Hall mobility was measured by using a standard van der Pauw configuration with four Au contacts, prepared as previously said, at the corners of a square configuration. The measurements were carried out using the same automatic acquisition system as for conductivity measure.

III. RESULTS

A. X-ray characterization

Figure 1 presents the x-ray diffraction spectra of deposited samples. Two distinct behaviors can be observed.

(a) For $1\% \leqslant f \leqslant 3\%$ the spectra show two well-defined peaks along [111] and [220] directions with a third one, but less resolved, along the [311] one. These peaks state the formation of a microcrystalline structure. Crystallite dimensions of these samples range between 130 and 200 Å in [220] direction and are almost constant to about 60 Å in the [111] one.

(b) For $f>3\%$ a very flat bump replaces the peak along the [111] direction, only for $f=4\%$ a small peak in [220] direction is detectable, indicating a dominant presence of an amorphous network in these samples. Thus, the increase in f causes a transition from the microcrystalline to the amorphous phase. In the following, the films deposited at $f \leqslant 3\%$ will be called microcrystalline and those deposited at $f>3\%$ amorphous, according to the electrical behavior, discussed in the following section.

B. Electrical conductivity

Electronic transport measurements carried out on the deposited samples evidenced a clear dependence on f. This fact can be explained in terms of a network structure change, as indicated by XRD measurements.

For the whole set of films, the electrical conductivity as a function of T, $\sigma(T)$, has been measured and heating-cooling cycles have been repeated. In microcrystalline samples, the

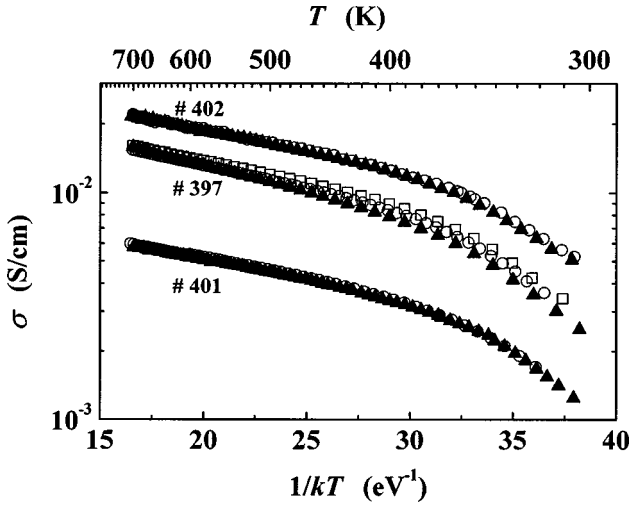

FIG. 2. Electrical conductivity curves for microcrystalline samples as a function of T, all carried out in the heating run. Triangles, first measurement; circles, second; squares, third.

$\sigma(T)$ curve obtained during a cooling run superimposes well with that measured during the heating one: at the end of the temperature cycle, all the experimental points practically lay on the same curve (Fig. 2). On the contrary, in amorphouslike specimens, we observe a thermal hysteresis effect with the $\sigma(T)$ values, for the heating run, lower than those for the cooling one. The $\sigma(T)$ hysteresis is open, i.e., RT $\sigma(T)$ values for the heating (starting point) and cooling (final point) significantly differ from each other. Depending on f, this difference can be up to one order of magnitude. As an example, in Fig. 3 a thermal cycle of sample 399 is reported.

Another experimental observation is the strong difference between the values of $\sigma(T)$ for microcrystalline and amorphous samples. At room temperature, $\sigma(T)$ varies of several orders of magnitude, being higher for microcrystalline specimens ($\simeq10^{-3}$ S cm^{-1}).

Some common features can be evidenced in all $\sigma(T)$ curves: the conductivity curves for microcrystalline and amorphous films are roughly similar, decreasing continuously as a function of $1/kT$. Two regions can be identified at

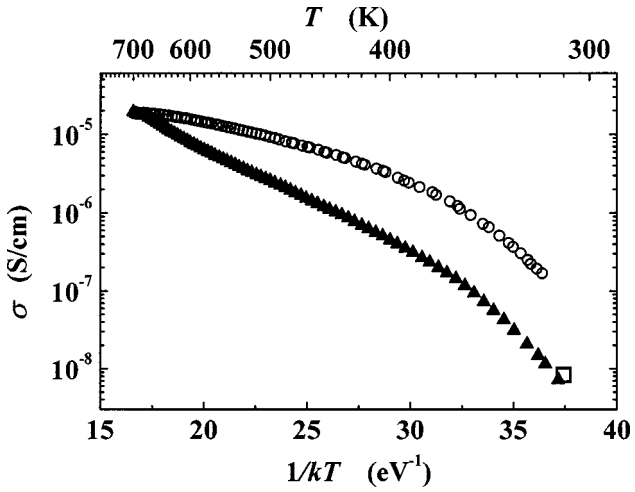

FIG. 3. Electrical conductivity curves for amorphous samples. Triangles, data collected during the heating run; circles, data for cooling run.

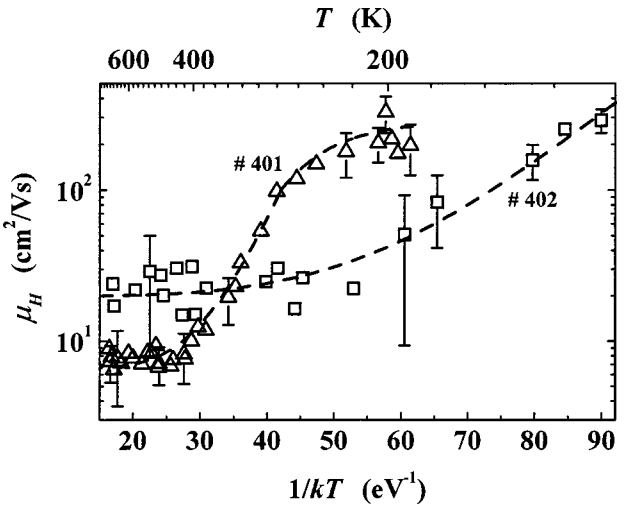

FIG. 4. Hall mobility as a function of the temperature for two microcrystalline specimens. Broken lines are only guides for eyes.

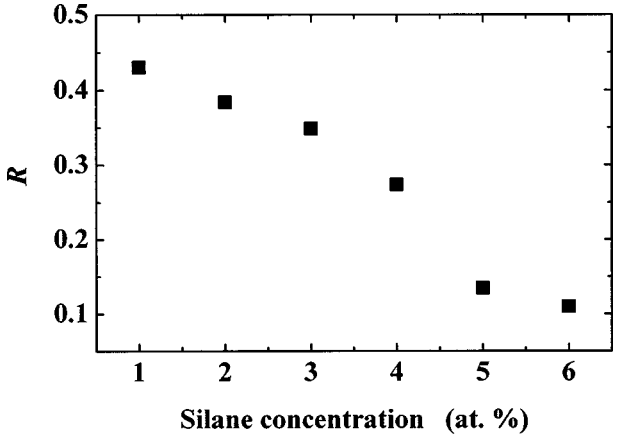

FIG. 5. Microstructure factor R vs silane concentration f for all the investigated samples.

high and low temperatures with very different activation energies, $E_{\sigma 1}$ and $E_{\sigma 2}$, respectively. For the investigated films, we observed that $E_{\sigma 1} < E_{\sigma 2}$. The mean activation energies are quoted in Table I, computed on all the thermal cycles. They are approximately constant in microcrystalline, $E_{\sigma 1} \approx 40$ meV and $E_{\sigma 2} \approx 140$ meV, and in amorphous samples $E_{\sigma 1} \approx 190$ meV and $E_{\sigma 2} \approx 600$ meV. The conductivities and the activation energies seem to be characteristic for a doped material. However, our samples are unintentionally doped and any doping source cannot be evidenced inside the deposition system. We think that these values are controlled by the density of states distribution linked to microstructure of the films and we will discuss later a possible model for these activation energies.

C. Hall mobility

Hall mobility as a function of the temperature $\mu_H(T)$ was computed from Hall coefficient measurements, carried out in the range 120–700 K. Figure 4 shows the $\mu_H(T)$ curves for two microcrystalline films. Their Hall coefficients are negative in the whole T range (conduction due to electrons).

The two $\mu_H(T)$ curves show a near constant behavior at temperature higher than $\approx$400 K for sample 401 and $\approx$230 K for sample 402. At these temperatures $\mu_H(T) \approx 7$ cm^2/V s for the sample 401, while increases to about 20 cm^2/V s in the sample 402. At temperatures lower than 400 K or 230 K, $\mu_H(T)$ shows a temperature dependent behavior with activation energy of $\approx$100 meV and $\approx$35 meV for sample 401 and 402, respectively. The highest measured $\mu_H(T)$ values are about 300 cm^2/V s at $T \approx 200$ K for sample 401 and $\approx$400 cm^2/V s at $T \approx 120$ K for film 402.

For amorphous films we were unable to measure any reliable value for $\mu_H(T)$.

IV. DISCUSSION

Before starting the discussion on the electrical transport properties, we have to remember some results on the hydrogen content, C_H. Its values, evaluated from IR absorption data,[6] reflect the transition from a microcrystalline to an amorphous network. In fact, C_H remains constant to $\approx$2 at. % for $1\% \leqslant f \leqslant 3\%$. At this last f value, C_H starts to increase attaining about 8 at. % when $f = 6\%$. This increase of C_H can be explained taking into account that the density of unsaturated bonds is higher in amorphous material than in microcrystalline one.

Moreover, the microstructure factor $R = I_{2100}/(I_{2000} + I_{2100})$ was calculated by fitting the two experimental absorption IR peaks at 2000 cm^{-1} (vibrational modes of SiH group) and 2100 cm^{-1} (vibrational modes of SiH_2 group) with two Gaussian shaped curves.[7,8] This allowed computing the integrated absorption areas, I_{2000} and I_{2100}, after the deconvolution procedure.

The microstructure factor R is plotted as a function of f in Fig. 5. The low R values, for $f > 4\%$, are associated with a high content of the monohydride group. An increase of R occurs for silane concentration below 4% when the films are microcrystalline. Then the mode near 2100 cm^{-1} can be associated to the presence of hydrogen and silicon bonds on grain boundaries.[9] This distribution of the hydrogen can be a possible explanation for the independence of the measured conductivity from the direction of the temperature run (Fig. 2). In fact, we can exclude crystallization according to the fact that the maximum value of the measured temperature (700 K) is higher of deposition temperature (620 K), but much lower than crystallization one (1100 K). The hydrogen on the outer walls of the islands can move, but not escape from the structure.

The samples used in this work differ from each other only for the f value (Table I), all the other deposition parameters being constant. The microcrystalline-amorphous transition at $f \approx 3\%$ can be linked to the physical-chemical processes at and near the outer growing surface. In fact, the deposition rate r shows a rapidly increasing behavior with f, leading to a progressively lack of ordering during the growth as the f rises. r is $\approx$0.37 Å s^{-1} when $f = 1\%$, increases to $\approx$0.85 Å s^{-1} for $f = 3\%$ and then rises less rapidly going to $\approx$1.3 Å s^{-1} when $f = 6\%$.

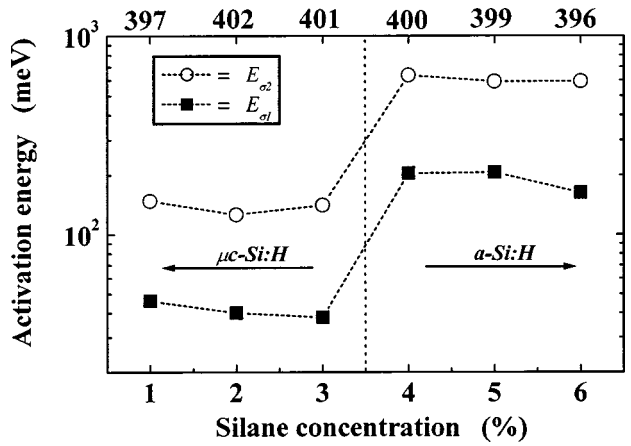

FIG. 6. Conductivity activation energies $E_{\sigma 1}$ and $E_{\sigma 2}$ plotted as a function of silane concentration. Average values are quoted. Top axis shows the sample number. Broken lines are only guides for eyes.

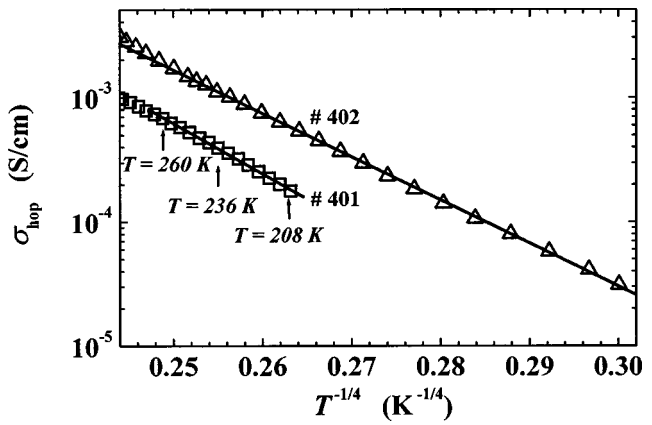

FIG. 7. Electrical conductivity plotted as a function of $T^{1/4}$ for samples 401 and 402. Continuous lines are best fits to the experimental data.

A. Electrical conduction

As pointed out in the Results, all samples show an activation energy at high temperature, $E_{\sigma 1}$, lower than $E_{\sigma 2}$, measured at low temperature.

This result can be explained in microcrystalline samples in the framework of the so-called two-phase model.[10] The model assumes that crystalline islands (a phase) are embedded in an interconnective tissue (the other phase). The prevailing electrical conduction is controlled by a phase or the other, according to the temperature and to the weight of each phase. Plotting $\ln[\sigma(T)]$ vs $1/T$ (Arrenius plot), the curve slope due to the tissue is always lower than that due to the islands: the two curves cross at a temperature depending on material and sample. Increasing the temperature, the prevailing conduction channel can be first in the tissue and, at the crossing point, it moves into the islands (upward kink). When the situation is reversed, first islands and then tissue, the kink is downward. The properties of each sample, and its history, are crucial for the prevalence of a case on the other.

All our samples show a downward kink, $E_{\sigma 1} < E_{\sigma 2}$, with a crossing temperature of $\approx 380-400$ K. This result allows stating that all specimens present a microcrystalline structure, even if not clearly evidenced by XRD. This means that in the so-called amorphous samples, the tissue is the prevailing phase, but even that the electrical transport is able to evidence a more fine structure.

Plotting $E_{\sigma 1}$ and $E_{\sigma 2}$ as a function of f (Fig. 6), we can observe that both activation energies have the same behavior: near constant up to $f=3\%$, with a clear transition to the higher values when $3\% < f < 4\%$. This result allows affirming that the structural and morphological properties of the two classes of films are largely homogeneous inside each f range.

In microcrystalline samples, according to the temperature range and to $E_{\sigma 1}$ and $E_{\sigma 2}$ values, the conduction is controlled by transitions between defect levels inside the energy gap and the conduction band. The sign of the Hall coefficient supports this last affirmation. The mean depth of the two defect bands, probably traps on the grain boundaries, is ≈ 35 meV and ≈ 150 meV, respectively. Assuming that the conduction current is controlled by thermionic emission,[11] with an intensity of the lowest current, $I_o = 10^{-9}$ A and $T = 330$ K, we obtain a barrier height of ≈ 170 meV, not far from our measured $E_{\sigma 2}$ values. 150–200 meV are the value quoted in the literature[12] for a trap density less than 10^{16} m^{-2}. Increasing trap density to about 3×10^{16} m^{-2}, the barrier height decreases to 30–35 meV. These trap levels can be identified with nonsaturated bonds and/or structural defects at the surface of the microcrystalline islands.

The presence of a high density of traps or defect levels at grain boundaries, affecting the density of state distribution at the Fermi level, seems to be in agreement with variable-range hopping transport, exhibited at low temperature. Indeed, on microcrystalline samples 401 and 402, a linear dependence of $\ln[\sigma(T)]$ on $T^{-1/4}$ is well evidenced below 230 K (Fig. 7). Using our experimental data for activation energy at low temperature, $E_{\sigma 1}$ (about 40 meV for sample 401 and 402) and standard relations for variable hopping regime as quoted in Mott's classical book, we were able to evaluate a density of state ranging between $10^{18}-10^{19}$ eV^{-1} cm^{-3} at the Fermi level.

The conductivity data for amorphous samples must be interpreted in a different way. First, we have to remember the strong difference between the values of $\sigma(T)$ for microcrystalline ($\cong 10^{-3}-10^{-2}$ S cm^{-1}) and amorphous samples ($\cong 10^{-8}-10^{-5}$ S cm^{-1}) at RT. The difference in the $\sigma(T)$ values maintains rather constant in the whole temperature range. According to the $\sigma(T)$ values for amorphous films, the conduction cannot be into extended states, but is among localized states inside the mobility gap. In fact, in these samples the optical gap, evaluated using the Tauc's approach, is ≈ 1.6 eV, being less for microcrystalline ones ($\approx 1.3-1.4$ eV). As a second point, we can observe that, in amorphous samples, the mean value of $E_{\sigma 1} \approx 190$ meV is not far from the average value of $E_{\sigma 2} \approx 140$ meV, measured in microcrystalline specimens (Table I). This result seems to support our previous affirmation that the so-called amorphous specimens have a two-phase (islands and interconnective tissue) micronetwork. In this sense, the quoted activation energies correspond to transitions from the same wide defect band inside the energy gap. As previously, the defects can be identified with trap states at the outer surface of islands.

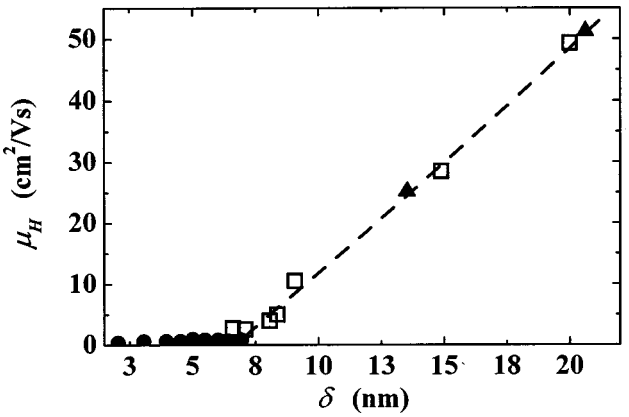

FIG. 8. Hall mobility as a function of island dimension δ. Triangles, this work; circles, after Ref. 13; squares, after Ref. 14.

The second activation energy $E_{\sigma 2} \approx 600$ meV can be attributed to transitions from localized states in the center of the energy gap towards localized states of the conduction band tail.

B. Hall mobility

The RT value of $\mu_H(T)$ is about 25 cm^2/V s and 50 cm^2/V s for sample 402 and 401, respectively. The average grain dimensions δ computed by using the [220] diffraction peak (Fig. 1) is $\approx$200 Å for sample 401 and $\approx$130 Å for sample 402. It is well known that $\mu_H(T)$ depends on δ, and follows a linear behavior when δ is higher than a critical value.[13] We plot the two $\mu_H(T)$ values as a function of δ (Fig. 8), comparing them with other experimental results.[13,14] As one can see, the agreement is very good, in this way supporting the assumption about a real microstructure of the films.

This result looks interesting for technological applications because the island dimensions can be controlled through a suitable choice of the deposition conditions.

C. Thermal hysteresis of the electrical conductivity

This effect is shown only by amorphous specimens (Fig. 3) and it has been described in the result section. Similar effects were found in amorphous silicon carbon (a-SiC:H) films below the crystallization temperature.[15–17] Thermal hysteresis is found even in case of multiple thermal cycles, but with a possible gradual reduction of the effect. As in case of a-SiC:H, we interpret this effect as due to rearrangements of H atoms in the amorphous tissue, the crystalline islands being much more stable. These metastability effects are well known.[18] They are studied, in general, measuring the change of the time constant for the hydrogen evolution. In fact, the conductivity is proportional to $\exp[(-t/\tau)^{\beta}]$ and a measure of the time constant τ and of the β exponent characterizes the hydrogen evolution process, increasing by steps the annealing temperature. Limited hydrogen evolution and absence of crystallization effects are demonstrated by the possibility to repeat the cycle without significant changes in the $\sigma(T)$ values. However, when the highest annealing temperature at the end of the heating cycle is approaching the crystallization limit,[19] the activation energies of the conductivity tends to decrease as a consequence of an evolution towards a more stable network.

V. CONCLUSIONS

We found that electrical properties of PECVD deposited silicon films strongly depend on the silane concentration f. The network structure of Si films is strongly affected by the range of this critical parameter. Electrical conductivity measurements as a function of temperature show two different activation energies in all investigated films. These results can be explained in the framework of the so-called two-phase model. The electrical transport data analysis is able to evidence microstructures also in the film with prevailing amorphous phase. Hall mobility at room temperature is linear function of the average grain dimensions and assumes the values of 50 cm^2/V s for sample with the highest crystallinity degree.

Some metastability effects of the conductivity can be explained as due to the movement of hydrogen atoms inside the amorphous phase and on the outer surface of the crystalline islands.

The control of the electrical properties by means of f can be usefully applied in the electronic devices fabrication.

ACKNOWLEDGMENTS

XRD measurements by C. Minarini (ENEA laboratory of Portici) are gratefully acknowledged. This work was supported by Istituto Nazionale di Fisica della Materia (INFM).

[1] S. Veprek and V. Malecek, Solid-State Electron. **11**, 683 (1968).
[2] J. Meier *et al.*, in *Proceedings of the 1998 Second World Conference on Photovoltaic Solar Energy Conversion*, edited by J. Schmid, H. A. Offenbrink, P. Helm, H. Ehmann, and E. D. Dunlop (Vienna, Austria, 1998), pp. 375–380; J. Meier, R. Fluckiger, H. Keppner, and A. Shah, Appl. Phys. Lett. **65**, 860 (1994).
[3] M. Mulato, Y. Chen, S. Wagner, and A. R. Zanatta, J. Non-Cryst. Solids **266-269**, 1260 (2000).
[4] P. Alpuim, V. Chu, and J. P. Conde, J. Appl. Phys. **86**, 3812 (1999).
[5] U. Coscia, G. Ambrosone, P. Maddalena, S. Lettieri, M. Ambrico, and C. Minarini, Thin Solid Films **403-404**, 130 (2002).
[6] G. Ambrosone, U. Coscia, S. Lettieri, and P. Maddalena, Mater. Sci. Eng., B **101**, 236 (2003).
[7] H. Wieder, M. Cardona, and C. R. Guarnieri, Phys. Status Solidi B **92**, 99 (1979).
[8] D. K. Basa and F. W. Smith, Thin Solid Films **193**, 121 (1990).
[9] Y. Mishima, S. Miyaaki, M. Hirose, and Y. Osaka, Philos. Mag. B **46**, 1 (1982); T. Itoh, K. Yamamoto, K. Ishikoshi, S. Nonomura, and S. Nitta, J. Non-Cryst. Solids **266-269**, 201 (2000).
[10] W. Paul and D. A. Anderson, Sol. Energy Mater. Sol. Cells **5**, 229 (1981); J. Kočka *et al.*, J. Non-Cryst. Solids **299-302**, 355 (2002); F. Liu, M. Zhu, Y. Feng, Y. Han, J. Liu, S. Kasouit, and R. Vanderhaghen, *ibid.* **299-302**, 385 (2002).
[11] J. W. Orton and M. J. Powell, Rep. Prog. Phys. **43**, 1263 (1980).
[12] R. Vanderhaghen, S. Kasouit, R. Benot, V. Chu, J. P. Conde, F. Liu, A. De Martino, and P. Roca i Cabarrocas, J. Non-Cryst. Solids **299-302**, 365 (2002).
[13] W. E. Spear, G. Willeke, and P. G. Le Comber, Physica B & C **117**, 908 (1983).
[14] V. Augelli and R. Murri, J. Non-Cryst. Solids **59-60**, 481 (1983).

[15]R. Murri, N. Pinto, G. Ambrosone, and U. Coscia, Phys. Rev. B **62**, 1801 (2000).
[16]R. Murri, N. Pinto, G. Ambrosone, U. Coscia, and P. Musto, J. Non-Cryst. Solids **299-302**, 902 (2002).
[17]R. Murri, N. Pinto, S. Giuliodori, G. Ambrosone, and U. Coscia, J. Mater. Sci.: Mater. Electron. **14**, 341 (2003).
[18]R. Meaudre, P. Jensen, and M. Meaudre, Phys. Rev. B **38**, 12449 (1988), and references therein.
[19]R. Bisaro, J. Magarino, Y. Pastol, P. German, and K. Zellama, Phys. Rev. B **40**, 7655 (1989).